The leukotriene biosynthesis inhibitor MK886 impedes DNA polymerase activity

Amit Ketkar[†], Maroof K. Zafar[†], Leena Maddukuri[†], Kinrin Yamanaka[§], Surajit Banerjee[‡], Martin Egli[ƒ], Jeong-Yun Choi[£], R. Stephen Lloyd[§] and Robert L. Eoff[†,]*

[†]Department of Biochemistry and Molecular Biology, University of Arkansas for Medical Sciences, Little Rock, AR 72205-7199, U.S.A.

[§]Center for Research on Occupational and Environmental Toxicology, Oregon Health & Science University, Portland, OR 97239, U.S.A.

[£]Department of Molecular Cell Biology, Samsung Biomedical Research Institute, Sungkyunkwan University School of Medicine, Suwon, Gyeonggi-do 440-746, Republic of Korea

[ƒ]Department of Biochemistry, Vanderbilt University, Nashville, TN 37232-0146, U.S.A.

[‡]Northeastern Collaborative Access Team and Department of Chemistry and Chemical Biology, Cornell University, Argonne National Laboratory, Argonne, IL 60439, U.S.A.

Address correspondence to:

Robert L. Eoff
Department of Biochemistry & Molecular Biology
University of Arkansas for Medical Sciences
4301 W. Markham St.
Little Rock, Arkansas 72205-7199
Telephone: (501) 686-8343
Fax: (501) 686-8169
E-mail: RLEOFF@UAMS.EDU

Running Title: Specificity and mechanism of DNA polymerase inhibition by MK886

SUPPORTING INFORMATION

CONTENTS

Table S1. Summary of molecular docking results of the Y-family DNA polymerases with MK886*.

PDB code	Dock Run	Pocket	Number of Clusters	FF Score of Top cluster
4EBC	1	A	23	-2021.93
(hpol ι)		B	7	-2020.93
		C	4	-2021.60
	2	A	22	-2015.89
		B	5	-2021.35
		C	8	-2019.35
	3	A	24	-2027.77
		B	7	-2023.57
		C	3	-2012.84
	4	A	24	-2019.57
		B	5	-2021.22
		C	5	-2019.42
	5	A	19	-2028.26
		B	8	-2021.26
		C	4	-2023.77
3MR2	1	A	29	-2499.42
(hpol η)		B	2	-2498.17
	2	A	31	-2495.30
		B	1	-2484.13
	3	A	25	-2498.66
		B	6	-2493.86
	4	A	29	-2496.03
		B	4	-2490.38
	5	A	27	-2499.60
		B	5	-2489.38
2OH2	1	A	29	-2017.98
(hpol κ)		B	2	-2003.41
	2	A	31	-2012.70
		B	0	-
	3	A	32	-2016.16
		B	0	-
	4	A	29	-2016.12
		B	4	-2005.19
	5	A	27	-2013.20
		B	5	-2005.36

*Five docking runs were performed with each of the three structures for Y-pols indicated by their PDB code in column 1, using coordinates of MK886 generated using Marvin Sketch. The resulting hits, or clusters of BMs were ranked based upon their individual FullFitness (FF) scores; the number of clusters localizing to each of the three binding pockets (A, B and C) for each docking run is indicated in column 4. The FF score for the top hit cluster from each docking run is given in the last column. The highest FF score for each pocket from all five docking runs is marked in blue.

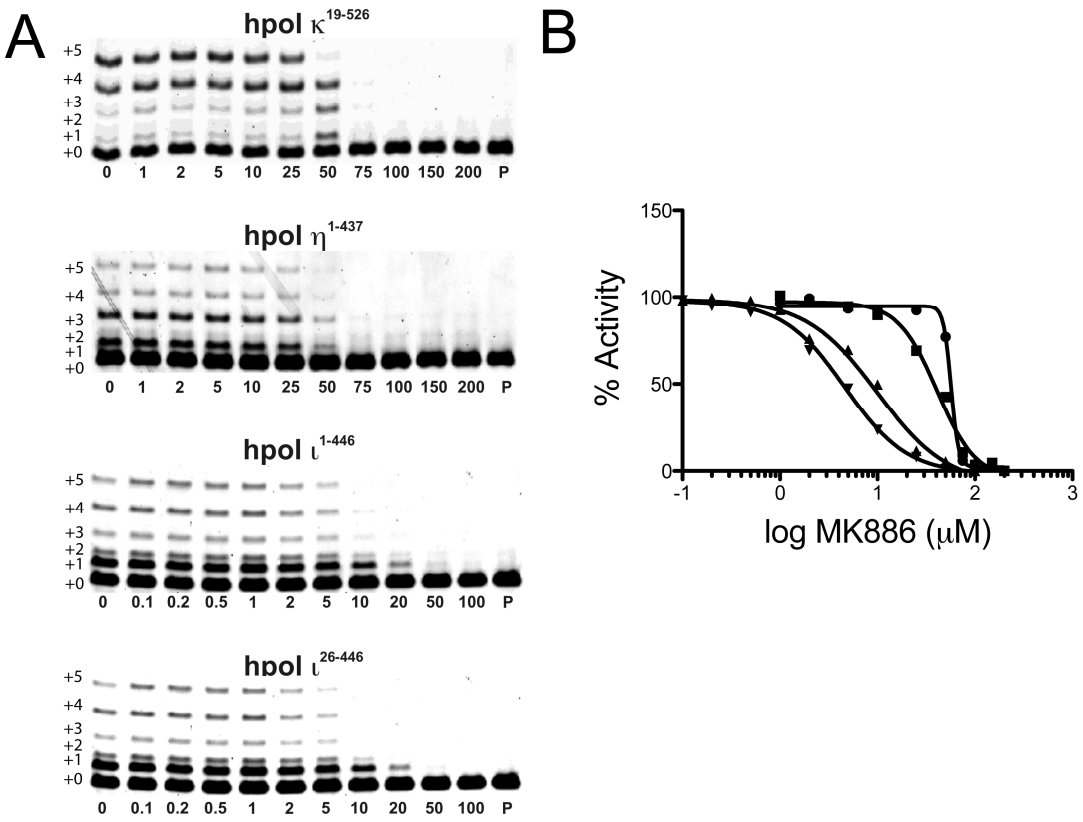

Figure S1. Determination of IC_{50} values for MK886 inhibition of Y-family DNA polymerases using a two minute time point. **A.** DNA polymerase-catalyzed primer extension assays were performed in the presence of increasing concentrations of MK886 with hpol κ^{19-526}, hpol η^{1-437}, hpol ι^{1-446} and hpol ι^{26-446} in the presence of all four dNTPs (0.25 mM) and $MgCl_2$ (5 mM). The concentration of MK886 (μM) is indicated underneath each lane. The un-reacted primer (P) was run as a control for each set of experiments. Extended polymerase products (+1 through +5) are indicated to the left of the gels. The reactions were allowed to proceed for 2 minutes. **B.** The IC_{50} values for MK886 inhibition of DNA polymerase activity were 56.8 ± 3.5 μM, 40.8 ± 9.5 μM, 10.0 ± 5.3 μM and 4.6 ± 1.2 μM for hpol κ^{19-526} (●), hpol η^{1-437} (■), hpol ι^{1-446} (▲) and hpol ι^{26-446} (▼), respectively.

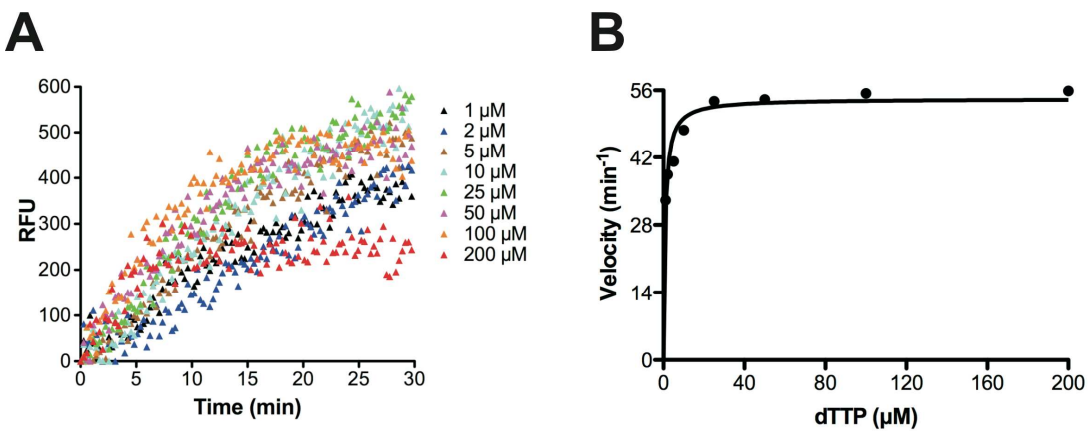

Figure S2. Reporter strand displacement assay to determine the mode of inhibition of hpol ι$^{26\text{-}446}$ by MK886. **A**. A Plot of relative fluorescence units (RFU) as a function of time is shown for a control experiment, conducted in the presence of 10% DMSO, in which the fluorescence signal from the TAMRA-labeled reporter displaced strand was measured directly at $\lambda_{emission}$ = 598 nm ($\lambda_{excitation}$ = 525 nm). The enzyme concentration was 5 nM, while that of the DNA substrate was 50 nM. As indicated, curves for each reaction performed at eight different concentrations of dTTP (between 1-200 μM as indicated in the plot legend) were plotted. Only the linear portion of each curve was considered when calculating the velocity at each dTTP concentration. **B**. Velocities obtained from **A** were plotted as a function of dTTP concentration, and fitted to a hyperbola, to obtain the steady state kinetic parameters (k_{cat} and $K_{M,dNTP}$).

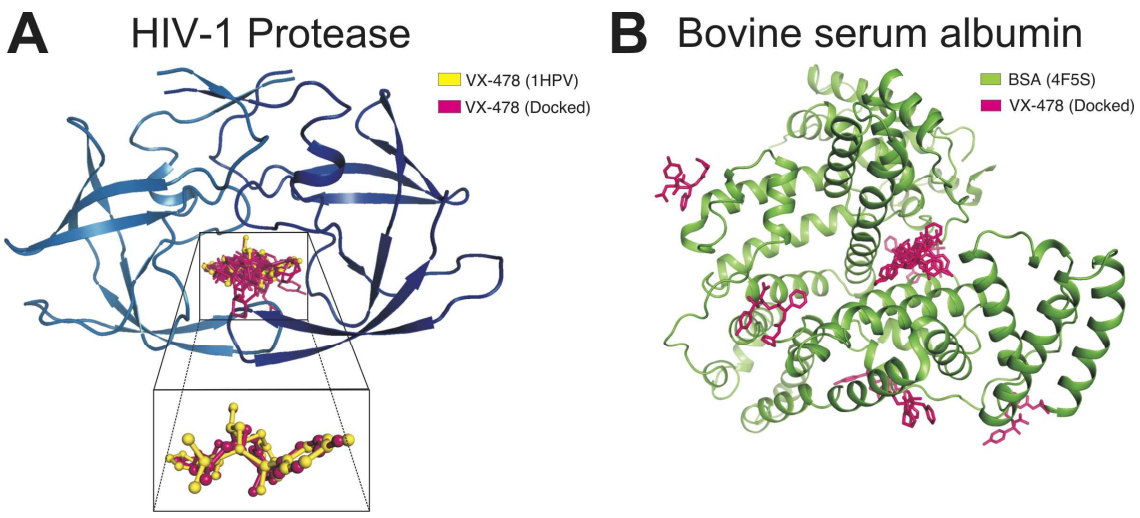

Figure S3. Docking analysis correctly identifies the small-molecule binding pocket of VX-478 on HIV-1 protease. **A**. Cartoon representation of the HIV-1 protease crystal structure (PDB file 1HPV) is shown; the two subunits of the dimer are colored *cyan* and *blue*. The *yellow* ball-and-stick model represents a molecule of the inhibitor VX478, as it is found in the crystal structure. The top 10 clusters of VX478 from a docking run are shown in *magenta*. The zoomed-out view shows the VX478 molecule from the crystal structure (*yellow*), and the top-scoring docked cluster (*magenta*), which superimposes almost perfectly on the crystal structure molecule. Note that all of the top 10 docked VX478 clusters bind in the close vicinity of the actual binding site seen in the crystal structure, with no outliers. **B.** Docking analysis with BSA (*green*, PDB code 4F5S) and VX-478 (*magenta*) reveals that the distribution of binding modes is scattered across the protein.

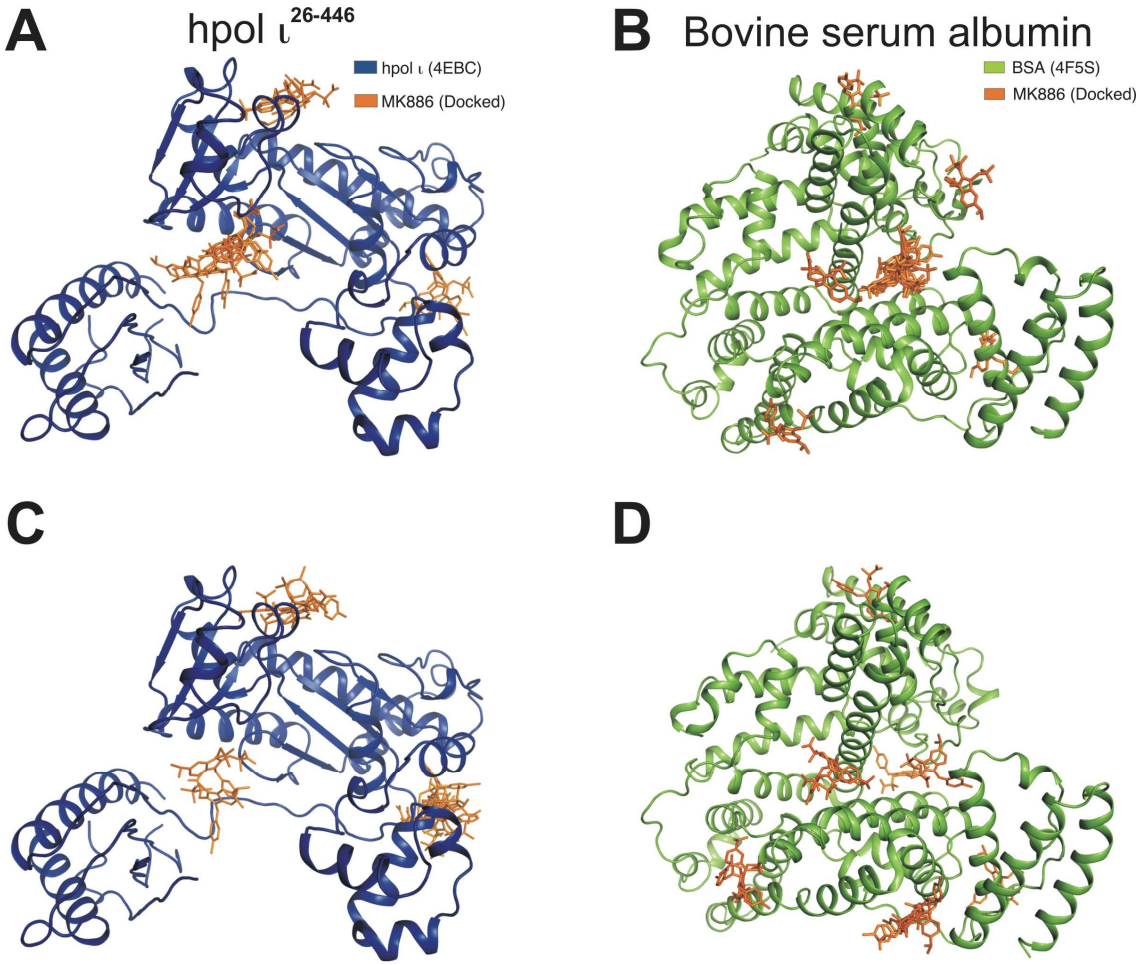

Figure S4. Docking analyses consistently identify MK886 binding pockets on hpol $\iota^{26\text{-}446}$ but appears to randomly position MK886 on BSA. **A.** SwissDock was used to dock MK886 onto the apo-form of hpol $\iota^{26\text{-}446}$ (PDB code 4EBC; *blue* cartoon). The top ten binding modes for MK886 (*orange*) from a single run are shown and all of them localize to one of the three pockets described in the main text. **B.** Docking was performed with MK886 (*orange*) and BSA (PDB code 4F5S; *green* cartoon). The top ten hits are distributed in a wide-ranging pattern across the protein. **C.** A second docking analysis was performed with MK886 and hpol $\iota^{26\text{-}446}$ using the exact same starting parameters as those in panel **A**. Again, the top ten binding modes are only observed in pockets A, B and C, which suggests that these sites on the polymerase are suitable for stable interactions with MK886. **D.** A second docking analysis with MK886 and BSA results in a panel of top hits that are distinctly different from those observed in the first run, suggesting that BSA does not have a specific binding pocket for MK886.

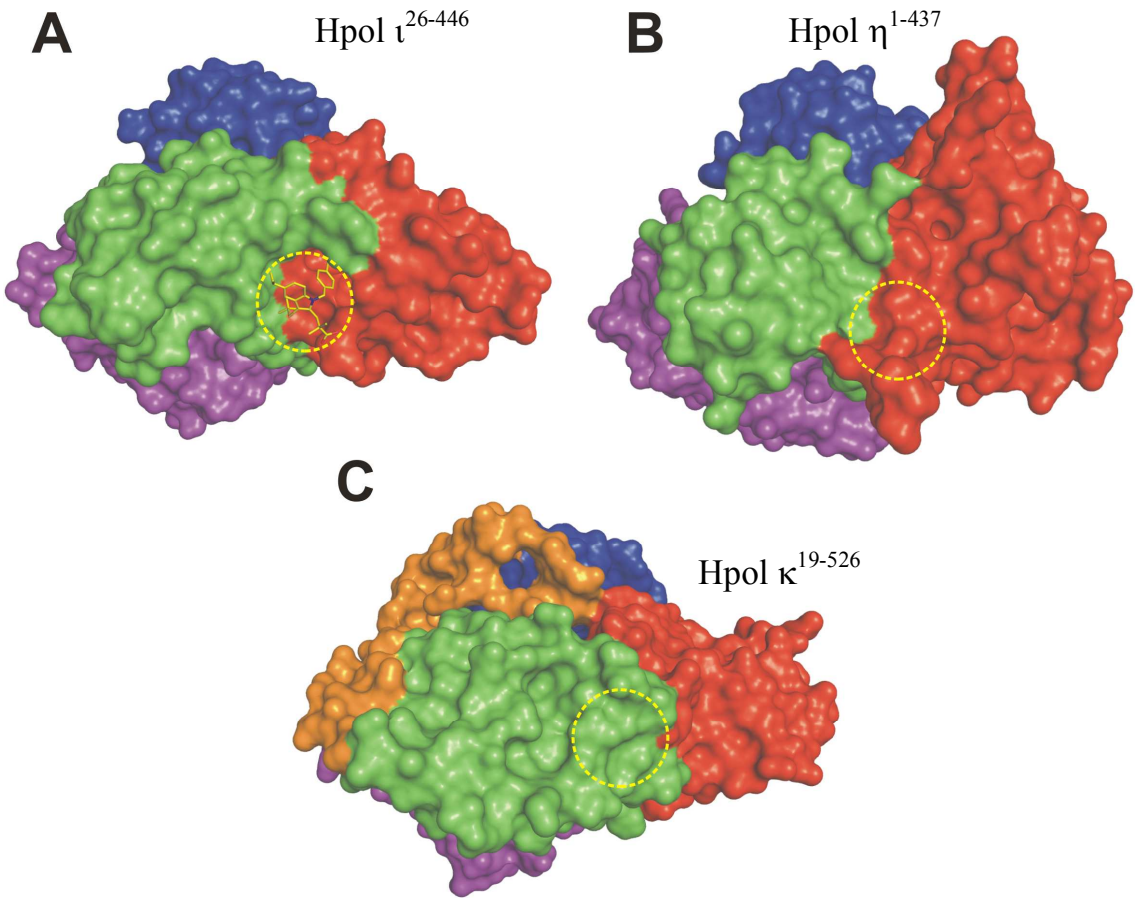

Figure S5. Comparison of MK886 binding pocket C in the Y-family DNA polymerases hpol ι^{26-446}, hpol η^{1-437} and hpol κ^{19-526}. Panels **A**, **B** and **C** show the surface representation of hpol ι^{26-446}, hpol η^{1-437} and hpol κ^{19-526} respectively, in the same relative orientation. Sub-domains are colored as earlier: Finger, *blue*; Thumb, *green*; Palm, *red* and little finger (or palm-associated domain), *purple*. The N-terminal clasp sub-domain in hpol κ^{19-526} is shown in *orange* in panel **C**. The dashed *yellow* circle marks the location of the MK886 binding pocket C in all enzymes. Pocket C is occupied by an MK886 molecule (shown as a stick model in **A**) only in hpol ι^{26-446}, while the corresponding 'pocket' in both hpol η^{1-437} and hpol κ^{19-526} is occluded by protein.